




## Article

# Photoswitchable Zirconium MOF for Light-Driven Hydrogen Storage

Vera V. Butova <sup>1,\*</sup>, Olga A. Burachevskaya <sup>1</sup>, Vitaly A. Podshibyakin <sup>2</sup>, Evgenii N. Shepelenko <sup>3</sup>,  
Andrei A. Tereshchenko <sup>1</sup>, Svetlana O. Shapovalova <sup>1</sup>, Oleg I. Il'in <sup>4</sup>, Vladimir A. Bren' <sup>2</sup>  
and Alexander V. Soldatov <sup>1</sup>

- <sup>1</sup> The Smart Materials Research Institute, Southern Federal University, Sladkova 178/24, 344090 Rostov-on-Don, Russia; oburachevskaya@sfedu.ru (O.A.B.); antereshenko@sfedu.ru (A.A.T.); scherkasova@sfedu.ru (S.O.S.); soldatov@sfedu.ru (A.V.S.)
- <sup>2</sup> Institute of Physical and Organic Chemistry, Southern Federal University, 344090 Rostov-on-Don, Russia; vpodshibakin@sfedu.ru (V.A.P.); vabren@sfedu.ru (V.A.B.)
- <sup>3</sup> Federal Research Center the Southern Scientific Center of the Russian Academy of Sciences, 344006 Rostov-on-Don, Russia; e-shepelenko@mail.ru
- <sup>4</sup> Institute of Nanotechnologies, Electronics and Equipment Engineering, Southern Federal University, Shevchenko 2, 347922 Taganrog, Russia; oiilin@sfedu.ru
- \* Correspondence: vbutova@sfedu.ru; Tel.: +7-863-297-51-28



**Citation:** Butova, V.V.; Burachevskaya, O.A.; Podshibyakin, V.A.; Shepelenko, E.N.; Tereshchenko, A.A.; Shapovalova, S.O.; Il'in, O.I.; Bren', V.A.; Soldatov, A.V. Photoswitchable Zirconium MOF for Light-Driven Hydrogen Storage. *Polymers* **2021**, *13*, 4052. <https://doi.org/10.3390/polym13224052>

Academic Editor: Muhammad Salahuddin Khan

Received: 9 November 2021

Accepted: 19 November 2021

Published: 22 November 2021

**Publisher's Note:** MDPI stays neutral with regard to jurisdictional claims in published maps and institutional affiliations.



**Copyright:** © 2021 by the authors. Licensee MDPI, Basel, Switzerland. This article is an open access article distributed under the terms and conditions of the Creative Commons Attribution (CC BY) license (<https://creativecommons.org/licenses/by/4.0/>).

**Abstract:** Here, we report a new photosensitive metal–organic framework (MOF) that was constructed via the modification of UiO-66-NH<sub>2</sub> with diarylethene molecules (DAE, 4-(5-Methoxy-1,2-dimethyl-1H-indol-3-yl)-3-(2,5-dimethylthiophen-3-yl)-4-furan-2,5-dione). The material that was obtained was a highly crystalline porous compound. The photoresponse of the modified MOF was observed via UV–Vis and IR spectroscopy. Most of the DAE molecules inside of the UiO-66-pores had an open conformation after synthesis. However, the equilibrium was able to be shifted further toward an open conformation using visible light irradiation with a wavelength of 520 nm. Conversely, UV-light with a wavelength of 450 nm initiated the transformation of the photoresponsive moieties inside of the pores to a closed modification. We have shown that this transformation could be used to stimulate hydrogen adsorption–desorption processes. Specifically, visible light irradiation increased the H<sub>2</sub> capacity of modified MOF, while UV-light decreased it. A similar hybrid material with DAE moieties in the UiO-66 scaffold was applied for hydrogen storage for the first time. Additionally, the obtained results are promising for smart H<sub>2</sub> storage that is able to be managed via light stimuli.

**Keywords:** UiO-66; smart material; diarylethene; UiO-66-NH<sub>2</sub>; photochromism; activation; FTIR; in situ IR-spectroscopy

## 1. Introduction

Metal–organic frameworks (MOFs) are porous materials that have recently attracted a great deal of attention due to their high-potential for use in molecule design [1,2]. These materials are constructed from inorganic clusters and organic molecules. The first ones tended to be designated as secondary building units (SBUs) [3]. They often contained one metal ion or a group of ions coordinated by oxygen or nitrogen from organic components, which are also known as linkers. Both SBUs and linkers define the geometry and functionality of the resulting framework. The introduction of functional groups via linker molecules results in the pore surface being decorated with them. Because of this, they are able to manipulate the properties of a material in the desired way. As a result, MOFs have been successfully applied in fields such as gas storage and separation [4,5], biomedicine [6,7], environmental remediation [8–10], and catalysis [11,12].

For modern devices, it is essential to control the material properties via external stimuli. Light is to be considered a preferred type of stimuli because it can be controlled precisely

in terms of both wavelength and radiation time [13]. In this way, imparting photoresponsive moieties to MOFs allows their fundamental properties to be managed. Different strategies have been applied to the design of new generations of photoswitchable MOFs. Photochromic molecules of a different nature have been introduced to MOFs [14]. Among other photochromic compounds, diarylethenes (DAEs) are one of the most promising due to their fatigue-resistant and thermally irreversible performance [15]. These molecules are able to reverse their configuration from that of a colorless open isomer to a colored closed form under UV-light irradiation. During this transformation, chemical bonds are formed between two heterocyclic thiophene groups. Visible light initiates a reverse process [16]. Generally, DAE molecules can be incorporated into the MOF scaffold in two ways: as parts of linker molecules [17–19] or as guests in the pores [20,21].

The photochromic process in DAE molecules affects the available pore volume, so it was applied for control adsorption and release of CO<sub>2</sub> [22–25] and gas separation [26–28] in previous studies. DAE molecules were introduced to MOFs to control the energy transfer process. Shustova and coauthors reported Zn-MOF with DAE and porphyrin species [29]. In this report, DAE was used to manage the fluorescence of porphyrin. Later Zhou and co-workers proposed a similar system to control the generation of singlet oxygen [30].

A list of MOFs was applied for targeted functionalization. One of the most popular MOFs for this purpose is UiO-66 and its derivatives. The main reason for its popularity is its stability and high porosity. UiO-66 is constructed from zirconium ions and terephthalate linkers. Each SBU in UiO-66 contains six Zr<sup>4+</sup> ions and bridge oxygen atoms and is able to be represented with a Zr<sub>6</sub>O<sub>4</sub>(OH)<sub>4</sub> formula unit (Figure 1). After the activation procedure, the bridge μ<sub>3</sub>-OH-group loses H<sup>+</sup>, and the SBU formula of the activated sample can be assigned to Zr<sub>6</sub>O<sub>6</sub>. This equilibrium process leads to UiO-66 and its derivatives presenting acidic properties [7,31,32]. Each SBU is coordinated with 12 linker molecules. High connectivity and strong covalent bonds result in the high stability of the UiO-66 scaffold. The introduction of functional groups into the terephthalate linker results in the functionalization of the pore surface, and it is repeatedly applied to manipulate the properties of MOF for use in desired applications [4,33,34].

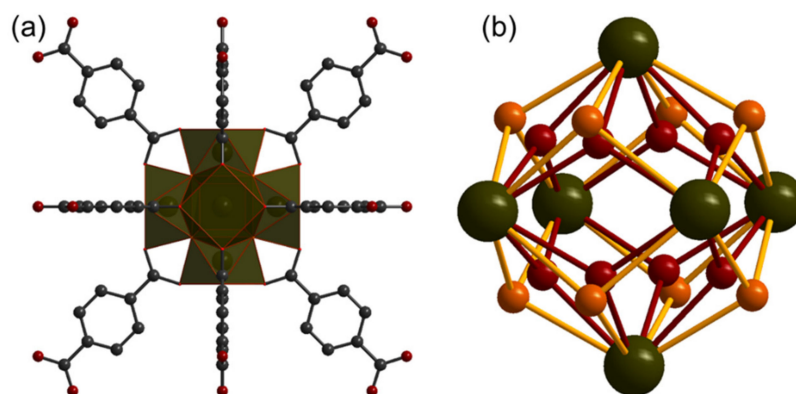


**Figure 1.** Schematic representation of the UiO-66 structure according to crystallographic data COD ID 4512072. (a) Dark green polyhedral represents the Zr-O cluster; gray spheres represent carbon atoms, dark red represents for oxygen. (b) Schematic representation of Zr<sub>6</sub>O<sub>4</sub>(OH)<sub>4</sub> SBU. Both oxygen positions are provided: μ<sub>3</sub>-O (dark red) and μ<sub>3</sub>-OH (orange). Oxygen atoms can alternate to occupy each of them The picture was prepared in Diamond, version 4.6.5.

Here, we report the synthesis procedure for the incorporation of DAE-molecules to the UiO-66-NH<sub>2</sub> framework. We used covalent the bonding of photoresponsive moieties and porous scaffolds to avoid the leakage of functional species.

## 2. Materials and Methods

### 2.1. Synthesis

The starting materials zirconium tetrachloride ( $ZrCl_4$ ), amino terephthalic acid ( $NH_2$ -BDC), benzoic acid (BA), N, N-dimethylformamide (DMF), and isopropanol were purchased from commercial suppliers and were used without further purification. Deionized water was obtained from the the Simplicity UV water purification system (Merck Millipore).

UiO-66- $NH_2$  was synthesized according to a previously reported technique [7]. Briefly,  $ZrCl_4$ ,  $NH_2$ -BDC, deionized water, and BA were completely dissolved in DMF. The molar ratio  $ZrCl_4$ :  $NH_2$ -BDC:  $H_2O$ : BA: DMF was 1: 1: 3: 10: 300. The reaction mixture was placed into a preheated oven and was held at 120 °C for 24 h. After being cooled, the precipitate was collected via centrifugation and was washed twice with DMF and with isopropanol. It was dried at 60 °C for 12 h.

The compound 4-(5-Methoxy-1,2-dimethyl-1H-indol-3-yl)-3-(2,5-dimethylthiophen-3-yl)-4-furan-2,5-dione (DAE) was obtained according to previously published procedures [35].

The modification of UiO-66- $NH_2$  was performed according to the following scheme (Figure 2).

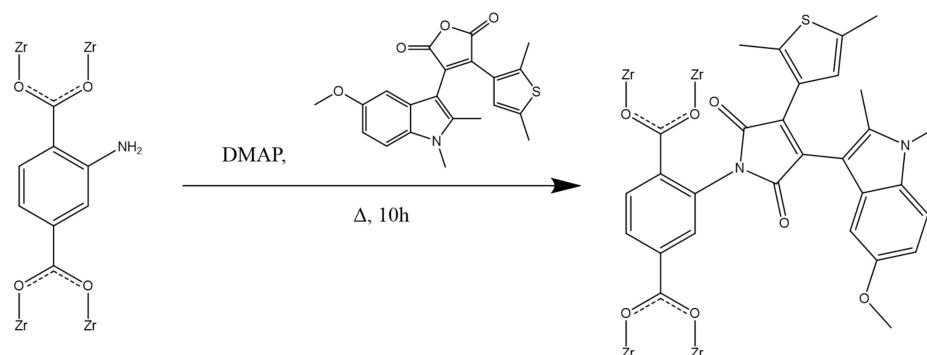


**Figure 2.** Scheme of UiO-66- $NH_2$  functionalization.

The modification of UiO-66- $NH_2$  was performed according to previously reported methods, with some modifications that were made based on the specific objective of obtaining diarylethenes with pyrrole-2,5-dione bridging fragments [35–37]. A solution containing 0.36 mmol of DAE in isopropyl alcohol (30 mL) was treated with UiO-66- $NH_2$  (0.06 mmol) and 4-dimethylaminopyridine (DMAP) (1 mg). The reaction mixture was refluxed for 10 h and cooled, and the solvent was removed by means of distillation. The resulting precipitate was washed with  $CH_2Cl_2$  until no staining was detected. The obtained sample was designated as DAE-UiO-66.

### 2.2. Methods

Powder X-ray diffraction (XRD) profiles were collected on an X-ray diffractometer Bruker D2 Phaser ( $CuK\alpha$ ,  $\lambda = 1.5417 \text{ \AA}$ ) with a scanning rate of 0.2 s/step and a step of  $0.01^\circ$ . Profile analysis was performed in Jana2006 software [38]. For X-ray fluorescence (XRF) analysis, we used the Bruker M4 Tornado. Thermogravimetric analysis (TGA) and differential scanning calorimetry (DSC) were performed using STA 449 F5 Jupiter in airflow.

A Nova Nanolab 600 scanning electron microscope (SEM) (FEI, Netherlands) was used for sample topological control. A Genesis SPECTRUM spectrometer (EDAX AMETEK, USA) was used for the elemental composition analysis, which was achieved through energy-dispersive X-ray spectroscopy (EDX). The EDX spectra were obtained with a 15 kV accelerating voltage and an 8.4 nA electron beam current. The signal accumulation time was 100 s.

$N_2$  and  $H_2$  adsorption–desorption isotherms were collected using an ASAP 2020 Accelerated Surface Area and Porosimetry analyzer (Micromeritics) at  $-196^\circ C$ . The samples were activated under a dynamic vacuum at  $90^\circ C$  for 12 h before measurements were taken.

To calculate the specific surface areas, we used N<sub>2</sub>-adsorption data and the BET model [39]. Pore size distribution is presented according to Non-Local Density Functional Theory (see details in Supplementary Materials). For the experiments with light-irradiation, we used two types of lasers—a green laser with a wavelength of 520 nm to trace the visible-light effects and a UV-laser with a wavelength 450 nm for the evaluation of the UV-light effects. The sample in the glass vessel was irradiated using the green laser and by emitting it through the glass for 10 min. We moved the laser point to avoid the excessive heating of the sample. The vessel was opened for irradiation with UV light, and the sample was treated with the UV light directly for 10 min. After this, the sample was closed and degassed at 50 °C for 2 h in a dynamic vacuum.

IR spectra were measured on a Bruker Vertex 70 spectrometer in DRIFT (Diffuse reflectance) geometry using an MCT detector and a Praying Mantis Low-Temperature Reaction Chamber (Harrick) attachment. The spectra were measured in the range from 5000 to 500 cm<sup>-1</sup> and had a resolution of 1 cm<sup>-1</sup> and scanning for 1 min for each spectrum. The reference sample was KBr powder. For sample activation, we used outgassing at 90 °C for 30 min and we then cooled the sample down to room temperature with further outgassing. After activating and recording initial spectra, both samples were irradiated with a green laser (520 nm) for 2 min, and the spectra were recorded under these stimuli.

UV-Vis spectra were collected on a UV-2600 (Shimadzu) spectrophotometer with an integrating sphere. The samples (14 mg) were mixed with BaSO<sub>4</sub> (300 mg), ground, mixed and pressed in the substrate vessel. After recording the initial spectra, samples were irradiated under a Newport lamp (power 500 W) with a filter passing 436 nm light for 10 min. After this, we recorded the spectra that were obtained from the treated samples.

### 3. Results

According to the XRD data, the UiO-66-NH<sub>2</sub> sample did not demonstrate a different crystal structure type after functionalization (Figure 3a). The SEM images also show that modification with the DAE-molecules did not affect the morphology of the particles (Figure 3b). The DAE-UiO-66 sample consisted of octahedral crystals that were 60–90 nm in size (Figure S1 in Supplementary Materials). EDX-mapping of the DAE-UiO-66 sample revealed the uniform distribution of Zr, C, N, and S atoms (Figure S2 in Supplementary Materials). Both of the UiO-66-NH<sub>2</sub> and DAE-UiO-66 samples had cubic symmetry with the Fm-3m (225) space group. However, profile analysis revealed that there was an increase in lattice constants, which increased from 20.794 Å (UiO-66-NH<sub>2</sub>) to 20.836 Å (DAE-UiO-66) (Figure S3, Tables S1 and S2 in Supplementary Materials). This could indicate stress in the framework of the DAE-UiO-66 sample due to the pores becoming filled with relatively photochromic molecules.

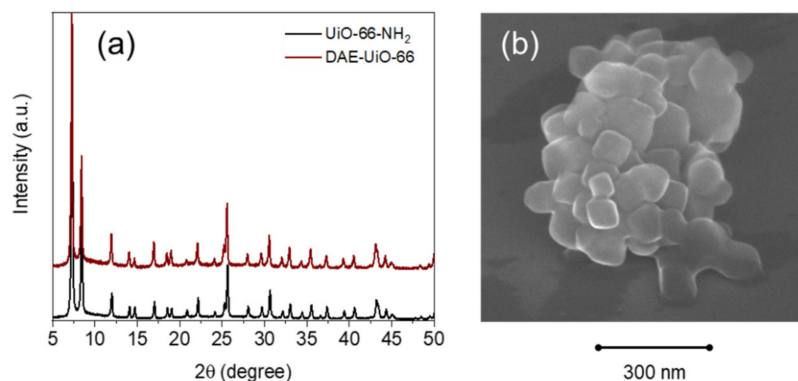
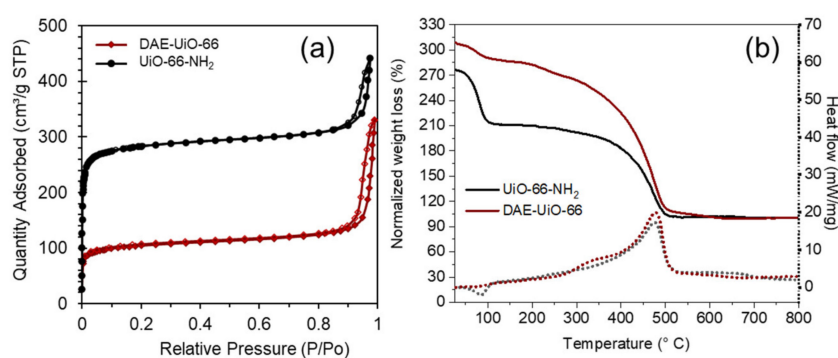


**Figure 3.** (a) XRD profiles of the UiO-66-NH<sub>2</sub> (black) and DAE-UiO-66 (brown) samples. Intensities are normalized and shifted along the *y*-axis for better representation. (b) SEM image of DAR-UiO-66 sample.

In good agreement with the XRD-data, we observed that the DAE-UiO-66 sample demonstrates lower porosity compared to the initial sample (Table 1). Figure 4a represents the nitrogen sorption isotherms of the UiO-66-NH<sub>2</sub> and DAE-UiO-66 samples. The shapes of both of the isotherms are associated with the microporous nature of the samples and can be assigned to type I as per IUPAC notification. Both isotherms demonstrate pronounced steps in the low-pressure region and a subsequent plateau due to the formation of a N<sub>2</sub> monolayer in the micropores. At relative pressures above 0.8, hysteresis loops of the H1 type could be observed, which is associated with the capillary condensation of nitrogen in cylindrical mesopores. The crystal structure of UiO-66-NH<sub>2</sub> contains two kinds of pores—tetrahedral and octahedral ones. The pore size distribution for the UiO-66-NH<sub>2</sub> and DAE-UiO-66 samples was calculated using the DFT method according to cylindrical pores (Figure S4, Table S1 in Supplementary Materials). It was shown that the small tetrahedral pores that were present on DAE-UiO-66 sample did not change in size compared to those found on the UiO-66-NH<sub>2</sub> sample, but the available volume of such pores was significantly reduced. While octahedral pores were present on the DAE-UiO-66 sample, their diameter was reduced. We suppose that this could indicate that photochromic molecules are located in octahedral pores, reducing their diameter. Tetrahedral pores are too small for such molecules, so they are empty, but most of them are blocked by photochromic molecules in the neighboring octahedral pores.

**Table 1.** Some properties of the synthesized samples UiO-66-NH<sub>2</sub> and DAE-UiO-66. SSA stands for the specific surface area. DAE content was calculated in mol %.

Samples' Designation	Unit Cell Parameters		Nitrogen Adsorption		TGA		XRF	
	a, Å	V, Å <sup>3</sup>	SSA, m <sup>2</sup> /g	Weight Loss, %	Molecular Weight	DAE Content	Zr:S:Cl	DAE Content
UiO-66-NH <sub>2</sub>	20.794(5)	8991(4)	1111	51.3	1519	-	6:0:3	-
DAE-UiO-66	20.836(6)	9046(5)	398	62.4	1945	9%	6:0.5:0.3	8%



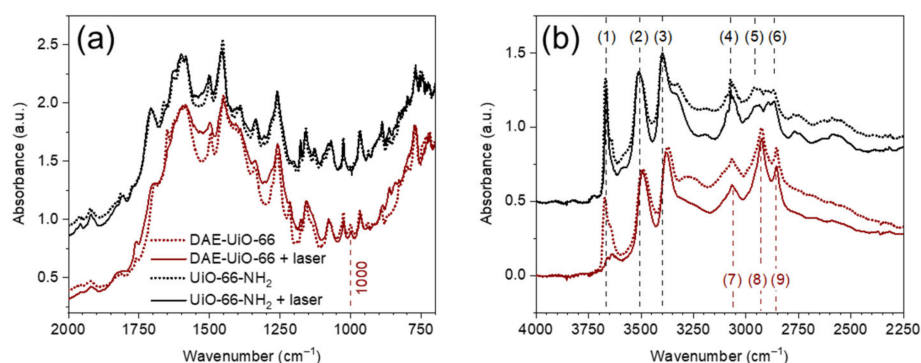
**Figure 4.** (a) Nitrogen adsorption–desorption isotherms of the UiO-66-NH<sub>2</sub> (black) and DAE-UiO-66 (brown) samples. Filled markers designate isotherm adsorption branches; empty markers represent desorption branches. (b) TGA (solid lines) and DSC (dashed lines) curves of UiO-66-NH<sub>2</sub> (black) and DAE-UiO-66 (brown) samples. TGA curve was normalized according to solid residual (see details in Figure S5 in Supplementary Materials).

Figure 4b represents the TGA and DSC curves for the UiO-66-NH<sub>2</sub> and DAE-UiO-66 samples. The TGA curves of both samples show two stages. The first weight loss occurs in the temperature range of 25–110 °C and is the result of the evacuation of water molecules from the porous MOFs. This process is endothermic and corresponds to negative peaks in the DSC curves. For the UiO-66-NH<sub>2</sub> sample, this step is more pronounced due to the higher porosity of the material before modification. The weight loss that occurs in the temperature range of 300–550 °C is associated with the decomposition of the organic parts

of frameworks and the resulting structural collapse. The TGA curves were normalized according to the amount of solid residual waste that remained after annealing the samples in the airflow. The interaction of both samples with oxygen from the air leads to the formation of six units of  $ZrO_2$  from each formula unit of the respective sample as the only solid residual. All organic components (linkers for the UiO-66-NH<sub>2</sub> sample and linkers and DAE-moieties for the DAE-UiO-66 sample) with oxygen form gaseous products. As such, the solid residual and weight loss of the samples could be recalculated in the composition of the materials (see Figure S5 in Supplementary Materials). Additional DAE-molecules in the UiO-66-scaffold led to more significant weight loss. Specifically, we calculated that one of each of the ten linkers in the DAE-UiO-66 sample was modified with the DAE-molecules (Table 1).

Additionally, we applied XRF analysis to quantify the amount of DAE molecules in the DAE-UiO-66. The unmodified UiO-66-NH<sub>2</sub> sample contains Zr and Cl in a molar ratio of 6:3. As previously reported, certain amino groups are able to interact with Cl<sup>-</sup> ions during synthesis due to the high acidity of the reaction mixture [40]. According to the XRF data, the formula unit of UiO-66-NH<sub>2</sub> could be represented as  $Zr_6O_4(OH)_4(C_8H_5O_4N)_3(C_8H_6O_4NCl)_3$ . The DAE-UiO-66 sample contains Zr, Cl, and S in a molar ratio of 6:0.3:0.5 (Table 1). Thus, the formula unit of DAE-UiO-66 is  $Zr_6O_4(OH)_4(C_8H_5O_4N)_{5.2}(C_8H_6O_4NCl)_{0.3}(C_{29}H_{23}O_7N_3S)_{0.5}$ . One octahedral pore is constructed from 12 linker molecules with 12 amino groups. According to the XRF data, one octahedral pore contains one DAE molecule. Moreover, we observed a reduction in the concentration of the -NH<sub>3</sub>Cl-moieties in the DAE-UiO-66 sample. This could indicate the formation of intermolecular bonds between DAE and the neighboring amino groups.

We traced the response of the synthesized compounds on the green laser with a wavelength 520 nm using FTIR spectroscopy (Figure 5). In the fingerprint region, both spectra are dominated by bands of the UiO-66-NH<sub>2</sub> framework. The only difference is a new mode at 1000 cm<sup>-1</sup> on the spectrum of the DAE-UiO-66 sample, which can be attributed to the C=C vibrations [41]. The as-synthesized samples contain a lot of adsorbed water molecules, which obstruct the interpretation of the far-infrared region of the spectrum. We evacuated the adsorbed water before conducting the measurements (Figure S6 in Supplementary Materials). Three specific bands were observed for the DAE-UiO-66 sample: at 3065, 2925, and 2853 cm<sup>-1</sup>, which are designated as (7), (8), and (9) in Figure 4b, respectively. We attributed them to the vibrations of the C-H bonds. The spectrum of the un-modified UiO-66-NH<sub>2</sub> sample contains a list of bands in this region, which are associated with the C-H vibrations of the linkers [7]. The amino group vibrations result in increases being present in the bands at 3510 and 3400 cm<sup>-1</sup> (lines (2) and (3) in Figure 5b) in the UiO-66-NH<sub>2</sub> spectrum [7,31]. The modification of the sample results in a shift of these modes to 3490 and 3370 cm<sup>-1</sup>, respectively. We attribute this to the involvement of this NH<sub>2</sub>-groups in the formation of bonds during modification. For activated samples, the modification effect on photo-response was traced. The UiO-66-NH<sub>2</sub> sample did not exhibit any significant response on laser irradiation, while the spectrum of the DAE-UiO-66 sample after irradiation contained a list of changes. The most pronounced one was an almost complete disappearance of band at 3670 cm<sup>-1</sup> (designated as (1) in Figure 5b). This band can be attributed to the vibrations of the μ<sub>3</sub>-OH groups in the UiO-66 framework. The deprotonation of such species results in a reduction in its intensity [31,34]. The band at 3330 cm<sup>-1</sup> in the UiO-66-NH<sub>2</sub> spectrum before irradiation refers to H-bonded water molecules [31,34]. After modification, the DAE-UiO-66 spectrum demonstrates the shift of this band to 3280 cm<sup>-1</sup> due to the formation of hydrogen bonds with more electronegative species [31]. We suppose that O=C-groups could form such bonds in a modified sample. After irradiation with a laser, the photochromic process affects the orientation of the molecules with the breaking of these bonds. In good agreement with this, we observed that the corresponding band vanished in the spectrum of the irradiated DAE-UiO-66.



**Figure 5.** FTIR spectra of UiO-66-NH<sub>2</sub> (black ones) and DAE-UiO-66 (brown ones) samples in the 700–2000 cm<sup>-1</sup> (a) and 2250–4000 cm<sup>-1</sup> (b) region. In both parts, spectra of the samples before laser irradiation are represented by dotted lines, while solid lines show spectra of the samples after 10 min of irradiation (wavelength 520 nm).

Figure 6a represents the UV–Vis spectra of the UiO-66-NH<sub>2</sub> and DAE-UiO-66 samples. After modification with the DAE molecules, the UiO-66-NH<sub>2</sub> spectrum preserved all of the characteristic features observed at 240, 265, and 375 nm. The introduction of DAE molecules resulted in three new modes at 220, 295, and 450 nm. This indicates that the DAE molecules were incorporated into the UiO-66-NH<sub>2</sub> structure in the open form [30]. The irradiation of the DAE-UiO-66 with UV-light gave rise to a new band at 545 nm (Figure 6b), which is in good agreement with the formation of a closed DAE-modification.

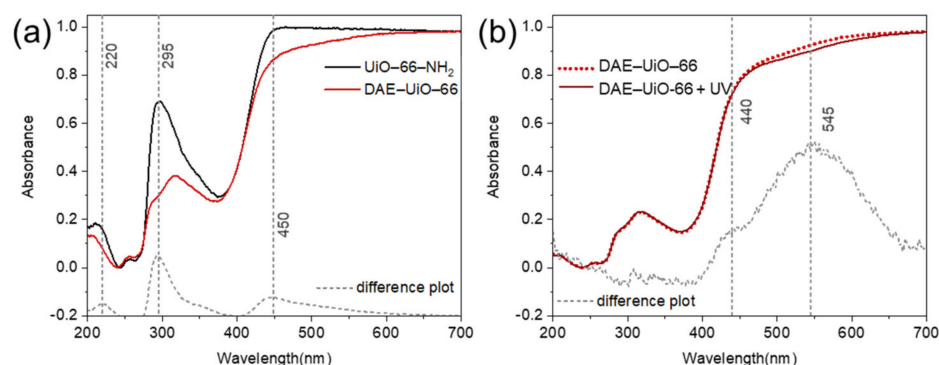


**Figure 6.** (a) UV–Vis spectra of samples UiO-66-NH<sub>2</sub> (black curve) and DAE-UiO-66 (red curve). (b) UV–Vis spectra of DAE-UiO-66 sample (dotted curve) and those after irradiation with light (436 nm) for 10 min (solid line). For both parts, difference plots are provided as dashed gray lines at the bottom.

We have traced the hydrogen capacity for the DAE-UiO-66 sample that was consistently irradiated with visible and UV light. The isotherms are presented in Figure 7a. After irradiation with visible light (wavelength 520 nm), the as-synthesized sample adsorbed 0.58 weight% of hydrogen at 77 K. This value is slightly higher than the H<sub>2</sub> capacity for the as-synthesized sample (0.55 weight%). Irradiation with UV-light (450 nm) reduced the hydrogen capacity. These changes are reversible because the same trend was reproduced after further irradiations with visible and UV light (Figure 7b). According to obtained data, we were able to conclude that the closed modification of the DAE molecules results in a lower pore volume being available than in an open modification. The same trend was reported for CO<sub>2</sub> adsorption [42] and C<sub>2</sub>H<sub>2</sub>/C<sub>2</sub>H<sub>4</sub> separation [27]. In order to trace the possible structural degradation after light stimulation, we measured the SSA for samples after each step. After the second irradiation with visible light, the SSA of the DAE-UiO-66 sample was estimated as 500 m<sup>2</sup>/g, indicating the porous structure of the framework without degradation (Supplementary Materials Figure S7). We also did not

observe any significant effect of light irradiation on the XRD patterns of the DAE-UiO-66 sample, indicating that transformations inside of the pores did not result in a structural collapse (Supplementary Materials Figure S8).

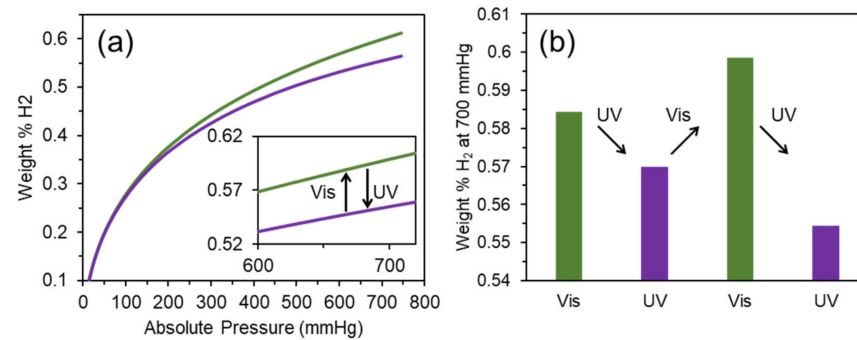


**Figure 7.** (a) Isotherms of hydrogen adsorption (77 K) for DAE-UiO-66 sample irradiated with visible light with a wavelength of 520 nm (green plot) and UV-light with a wavelength of 450 nm (violet plot). (b) Diagram of changing in H<sub>2</sub> capacity during sequential irradiation with visible light with a wavelength of 520 nm (green columns) and UV-light with a wavelength of 450 nm (violet columns).

#### 4. Discussion

According to the experimental data, we propose that the DAE molecules undergo the following transformations inside of the pores (Figure 8): After the synthesis, most of the DAE molecules are in the “open” modification, as confirmed by UV–Vis spectra. After irradiation with visible light, this equilibrium strongly shifts to the left, resulting in the open form being the dominant DAE modification. The open form increased hydrogen capacity and resulted in pronounced changes in the IR spectrum. According to the last experiment, irradiation with light (520 nm) led to a proton transfer from the  $\mu_3$ -OH group of the SBU in DAE-UiO-66. We attribute this transfer to the presence of DAE molecules inside of the pores because it was not observed in the non-modified UiO-66-NH<sub>2</sub> sample. It has been reported that the DAE molecules cannot be protonated in an acidic medium [43,44]. We suppose that the C=O groups of the DAE molecules could coordinate the H<sup>+</sup> ions. This transfer was promoted due to open conformation, allowing the  $\mu_3$ -OH groups to be close to the SBU and C=O groups of the DAE molecules. Under UV-irradiation, the DAE molecules underwent a “closed” modification, which was determined according to UV–Vis spectroscopy. Additionally, this resulted in the DAE-UiO-66 sample having a lower H<sub>2</sub> capacity.

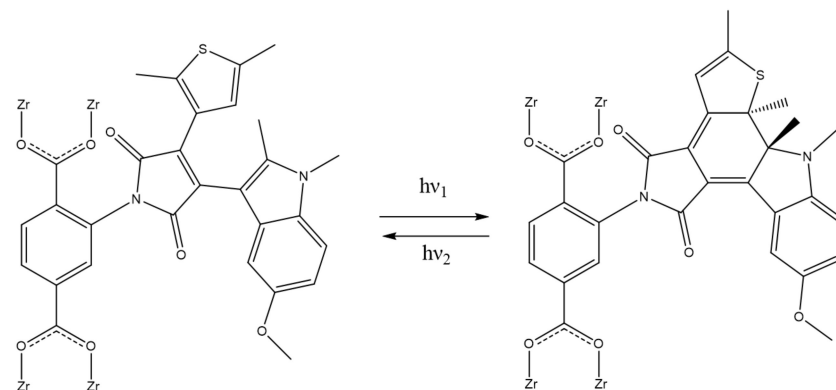


**Figure 8.** Scheme of DAE transformations inside DAE-UiO-66 pores under UV-light ( $h\nu_1$ ) and visible light ( $h\nu_2$ ).



## 5. Conclusions

In summary, we modified UiO-66-NH<sub>2</sub> with the photoactive DAE molecule 4-(5-Methoxy-1,2-dimethyl-1H-indol-3-yl)-3-(2,5-dimethylthiophen-3-yl)-4-furan-2,5-dione. These DAE molecules were used to modify the MOF scaffold for the first time. Moreover, the DAE moieties were incorporated into the linker of the canonical MOF, UiO-66NH<sub>2</sub>. The obtained material was highly crystalline and was isostructural to the initial UiO-66-NH<sub>2</sub> scaffold. However, we noticed an increase in the lattice constants, which was caused by stress due to the molecules in the pores. However, the obtained material, DAE-UiO-66, demonstrated a preserved porous structure, and its SSA was estimated to be almost 400 m<sup>2</sup>/g. According to a complex analysis of the IR-spectra, UV-Vis spectra, and hydrogen adsorption isotherms, we can conclude that the as-modified sample contained a mixture of two forms of DAE-molecules—"open" and "closed". The equilibrium was shifted to the "open" modification from the very beginning. However, some changes could be observed after the irradiation of DAE-UiO-66 with a visible light source, initiating the transformation of the DAE fillers in the pores to the open conformation. This increased the hydrogen capacity. Secondly, we observed the transport of protons from the μ<sub>3</sub>-OH groups of UiO-SBUs to the C=O groups of the DAE-molecules. Such a phenomenon was only able to be observed after the activation of MOF in dry air. The open-close transformations were also confirmed via UV-Vis spectroscopy. Finally, we measured the hydrogen capacity under UV/Vis irradiation and observed a reversible process that was able to be managed via light stimuli. Specifically, visible light increases the H<sub>2</sub> capacity, while UV-irradiation decreases it. We suppose that this result is an important step in the development of smart hydrogen storage with light-induced safe H<sub>2</sub>-desorption.

**Supplementary Materials:** The following are available online at <https://www.mdpi.com/article/10.3390/polym13224052/s1>, Figure S1: Representative SEM image of DAE-UiO-66 sample (a) and particle size distribution according to SEM data (b). Figure S2: EDX-mapping of DAE-UiO-66 sample. Figure S3: Experimental (black) and calculated (yellow) profiles of synthesized UiO-66-NH<sub>2</sub> (a) and DAE-UiO-66 (b) samples from fitting in Jana2006. Vertical lines indicate calculated pick positions. Difference plots are provided at the bottom of each picture, Figure S4: (a) BET surface area plot. (b) Low-pressure region of nitrogen adsorption isotherms. (c) Pore size distribution. (d) Experimental data and model fit of nitrogen adsorption isotherms that were used for pore-size distribution calculations, Figure S5: TGA (solid lines) and DTG (dotted lines) curves of UiO-66-NH<sub>2</sub> (a) and DAE-UiO-66 (b) samples. Dashed lines represent exact values of weight losses, which were used for calculations. Figure S6: FTIR spectra of as-synthesized samples and those after activation: UiO-66-NH<sub>2</sub> (a) and DAE-UiO-66 (b), Figure S7: Nitrogen adsorption-desorption isotherms of DAE-UiO-66 sample under sequential irradiation with visible light (520 nm, green plots) and UV-light (450 nm, violet plot). Filled markers designate isotherm adsorption branches; empty markers represent desorption branches. Figure S8: Powder XRD patterns of the samples UiO-66-NH<sub>2</sub> (black dotted line), DAE-UiO-66 (solid red line), and DAE-UiO-66 irradiated with visible light with wavelength 520 nm (solid green line), and DAE-UiO-66 irradiated with UV-light with a wavelength of 450 nm after irradiation with visible light (solid violet line). Part (a) demonstrates all 2θ range of profiles, while part (b) represents the magnification of the region 15–20 degrees. Table S1: Details of profile analysis, Table S2: Details of calculations according to nitrogen adsorption isotherm of UiO-66-NH<sub>2</sub> and DAE-UiO-66 samples.

**Author Contributions:** Conceptualization, V.V.B. and A.V.S.; methodology, O.A.B. and V.A.P.; validation, O.A.B., V.A.P. and E.N.S.; formal analysis, O.I.I., A.A.T. and S.O.S.; investigation, A.A.T.; resources, V.A.B.; writing—original draft preparation, V.V.B.; supervision, A.V.S. All authors have read and agreed to the published version of the manuscript.

**Funding:** The reported study was funded by the RFBR according to the research project № 18-29-04053.

**Institutional Review Board Statement:** Not applicable.

**Informed Consent Statement:** Not applicable.

**Data Availability Statement:** Data is contained within the article and Supplementary Materials.

**Conflicts of Interest:** The authors declare no conflict of interest.

## References

1. Yaghi, O.M.; O’Keeffe, M.; Ockwig, N.W.; Chae, H.K.; Eddaoudi, M.; Kim, J. Reticular synthesis and the design of new materials. *Nature* **2003**, *423*, 705–714. [[CrossRef](#)] [[PubMed](#)]
2. Butova, V.V.; Soldatov, M.A.; Guda, A.A.; Lomachenko, K.A.; Lamberti, C. Metal-organic frameworks: Structure, properties, methods of synthesis and characterization. *Russ. Chem. Rev.* **2016**, *85*, 280–307. [[CrossRef](#)]
3. Tranchemontagne, D.J.; Mendoza-Cortes, J.L.; O’Keeffe, M.; Yaghi, O.M. Secondary building units, nets and bonding in the chemistry of metal-organic frameworks. *Chem. Soc. Rev.* **2009**, *38*, 1257–1283. [[CrossRef](#)] [[PubMed](#)]
4. Butova, V.V.; Budnyk, A.P.; Charykov, K.M.; Vetlitsyna-Novikova, K.S.; Bugaev, A.L.; Guda, A.A.; Damin, A.; Chavan, S.M.; Oien-Odegaard, S.; Lillerud, K.P.; et al. Partial and Complete Substitution of the 1,4-Benzenedicarboxylate Linker in UiO-66 with 1,4-Naphthalenedicarboxylate: Synthesis, Characterization, and H<sub>2</sub>-Adsorption Properties. *Inorg. Chem.* **2019**, *58*, 1607–1620. [[CrossRef](#)]
5. Polyakov, V.A.; Butova, V.V.; Erofeeva, E.A.; Tereshchenko, A.A.; Soldatov, A.V. MW Synthesis of ZIF-7. The Effect of Solvent on Particle Size and Hydrogen Sorption Properties. *Energies* **2020**, *13*, 6306. [[CrossRef](#)]
6. Gorban, I.E.; Soldatov, M.A.; Butova, V.V.; Medvedev, P.V.; Burachevskaya, O.A.; Belanova, A.; Zolotukhin, P.; Soldatov, A.V. L-Leucine Loading and Release in MIL-100 Nanoparticles. *Int. J. Mol. Sci.* **2020**, *21*, 9758. [[CrossRef](#)]
7. Butova, V.V.; Burachevskaya, O.A.; Muratidi, M.A.; Surzhikova, I.I.; Zolotukhin, P.V.; Medvedev, P.V.; Gorban, I.E.; Kuzharov, A.A.; Soldatov, M.A. Loading of the Model Amino Acid Leucine in UiO-66 and UiO-66-NH<sub>2</sub>: Optimization of Metal-Organic Framework Carriers and Evaluation of Host-Guest Interactions. *Inorg. Chem.* **2021**, *60*, 5694–5703. [[CrossRef](#)]
8. Butova, V.V.; Polyakov, V.A.; Budnyk, A.P.; Aboraia, A.M.; Bulanova, E.A.; Guda, A.A.; Reshetnikova, E.A.; Podkovyrina, Y.S.; Lamberti, C.; Soldatov, A.V. Zn/Co ZIF family: MW synthesis, characterization and stability upon halogen sorption. *Polyhedron* **2018**, *154*, 457–464. [[CrossRef](#)]
9. Butova, V.V.; Bulanova, E.A.; Polyakov, V.A.; Guda, A.A.; Aboraia, A.M.; Shapovalov, V.V.; Zahran, H.Y.; Yahia, I.S.; Soldatov, A.V. The effect of cobalt content in Zn/Co-ZIF-8 on iodine capping properties. *Inorg. Chim. Acta* **2019**, *492*, 18–22. [[CrossRef](#)]
10. Butova, V.V.; Polyakov, V.A.; Erofeeva, E.A.; Yahia, I.S.; Zahran, H.Y.; Abd El-Rehim, A.F.; Aboraia, A.M.; Soldatov, A.V. Modification of ZIF-8 with triethylamine molecules for enhanced iodine and bromine adsorption. *Inorg. Chim. Acta* **2020**, *509*, 5. [[CrossRef](#)]
11. Van Velthoven, N.; Henrion, M.; Dallenes, J.; Krajnc, A.; Bugaev, A.L.; Liu, P.; Bals, S.; Soldatov, A.; Mali, G.; De Vos, D.E. S,O-Functionalized Metal-Organic Frameworks as Heterogeneous Single-Site Catalysts for the Oxidative Alkenylation of Arenes via C-H activation. *ACS Catal.* **2020**, *10*, 5077–5085. [[CrossRef](#)]
12. Braglia, L.; Borfecchia, E.; Maddalena, L.; Oien, S.; Lomachenko, K.A.; Bugaev, A.L.; Bordiga, S.; Soldatov, A.V.; Lillerud, K.P.; Lamberti, C. Exploring structure and reactivity of Cu sites in functionalized UiO-67 MOFs. *Catal. Today* **2017**, *283*, 89–103. [[CrossRef](#)]
13. Gui, B.; Meng, Y.; Xie, Y.; Du, K.; Sue, A.C.H.; Wang, C. Immobilizing Organic-Based Molecular Switches into Metal-Organic Frameworks: A Promising Strategy for Switching in Solid State. *Macromol. Rapid Commun.* **2018**, *39*. [[CrossRef](#)]
14. Castellanos, S.; Kapteijn, F.; Gascon, J. Photoswitchable metal organic frameworks: Turn on the lights and close the windows. *Crystengcomm* **2016**, *18*, 4006–4012. [[CrossRef](#)]
15. Huang, S.L.; Hor, T.S.A.; Jin, G.X. Photodriven single-crystal-to-single-crystal transformation. *Coord. Chem. Rev.* **2017**, *346*, 112–122. [[CrossRef](#)]
16. Rice, A.M.; Martin, C.R.; Galitskiy, V.A.; Berseneva, A.A.; Leith, G.A.; Shustova, N.B. Photophysics Modulation in Photoswitchable Metal-Organic Frameworks. *Chem. Rev.* **2020**, *120*, 8790–8813. [[CrossRef](#)]
17. Fan, C.B.; Liu, Z.Q.; Gong, L.L.; Zheng, A.M.; Zhang, L.; Yan, C.S.; Wu, H.Q.; Feng, X.F.; Luo, F. Photoswitching adsorption selectivity in a diarylethene-azobenzene MOF. *Chem. Commun.* **2017**, *53*, 763–766. [[CrossRef](#)]
18. Hu, X.G.; Li, X.L.; Yang, S.I. Novel photochromic infinite coordination polymer particles derived from a diarylethene photoswitch. *Chem. Commun.* **2015**, *51*, 10636–10639. [[CrossRef](#)]
19. Walton, I.M.; Cox, J.M.; Benson, C.A.; Patel, D.G.; Chen, Y.S.; Benedict, J.B. The role of atropisomers on the photo-reactivity and fatigue of diarylethene-based metal-organic frameworks. *New J. Chem.* **2016**, *40*, 101–106. [[CrossRef](#)]
20. Li, Z.Q.; Wang, G.N.; Ye, Y.X.; Li, B.; Li, H.R.; Chen, B.L. Loading Photochromic Molecules into a Luminescent Metal-Organic Framework for Information Anticounterfeiting. *Angew. Chem.-Int. Edit.* **2019**, *58*, 18025–18031. [[CrossRef](#)]
21. Schwartz, H.A.; Schaniel, D.; Ruschewitz, U. Tracking the light-induced isomerization processes and the photostability of spiropyrans embedded in the pores of crystalline nanoporous MOFs via IR spectroscopy. *Photochem. Photobiol. Sci.* **2020**, *19*, 1433–1441. [[CrossRef](#)] [[PubMed](#)]
22. Luo, F.; Fan, C.B.; Luo, M.B.; Wu, X.L.; Zhu, Y.; Pu, S.Z.; Xu, W.Y.; Guo, G.C. Photoswitching CO<sub>2</sub> Capture and Release in a Photochromic Diarylethene Metal-Organic Framework. *Angew. Chem.-Int. Edit.* **2014**, *53*, 9298–9301. [[CrossRef](#)] [[PubMed](#)]
23. Gong, L.L.; Feng, X.F.; Luo, F. Novel azo-Metal-Organic Framework Showing a 10-Connected bct Net, Breathing Behavior, and Unique Photoswitching Behavior toward CO<sub>2</sub>. *Inorg. Chem.* **2015**, *54*, 11587–11589. [[CrossRef](#)] [[PubMed](#)]
24. Lyndon, R.; Konstas, K.; Evans, R.A.; Keddle, D.J.; Hill, M.R.; Ladewig, B.P. Tunable Photodynamic Switching of DArE@PAF-1 for Carbon Capture. *Adv. Funct. Mater.* **2015**, *25*, 4405–4411. [[CrossRef](#)]

25. Huang, R.H.; Hill, M.R.; Babarao, R.; Medhekar, N.V. CO<sub>2</sub> Adsorption in Azobenzene Functionalized Stimuli Responsive Metal-Organic Frameworks. *J. Phys. Chem. C* **2016**, *120*, 16658–16667. [[CrossRef](#)]
26. Cox, J.M.; Walton, I.M.; Benedict, J.B. On the design of atropisomer-separable photochromic diarylethene-based metal-organic framework linkers. *J. Mater. Chem. C* **2016**, *4*, 4028–4033. [[CrossRef](#)]
27. Fan, C.B.; Gong, L.L.; Huang, L.; Luo, F.; Krishna, R.; Yi, X.F.; Zheng, A.M.; Zhang, L.; Pu, S.Z.; Feng, X.F.; et al. Significant Enhancement of C<sub>2</sub>H<sub>2</sub>/C<sub>2</sub>H<sub>4</sub> Separation by a Photochromic Diarylethene Unit: A Temperature- and Light-Responsive Separation Switch. *Angew. Chem.-Int. Edit.* **2017**, *56*, 7900–7906. [[CrossRef](#)]
28. Furlong, B.J.; Katz, M.J. Bistable Dithienylethene-Based Metal-Organic Framework Illustrating Optically Induced Changes in Chemical Separations. *J. Am. Chem. Soc.* **2017**, *139*, 13280–13283. [[CrossRef](#)]
29. Williams, D.E.; Rietman, J.A.; Maier, J.M.; Tan, R.; Greytak, A.B.; Smith, M.D.; Krause, J.A.; Shustova, N.B. Energy Transfer on Demand: Photoswitch-Directed Behavior of Metal-Porphyrin Frameworks. *J. Am. Chem. Soc.* **2014**, *136*, 11886–11889. [[CrossRef](#)]
30. Park, J.; Feng, D.W.; Yuan, S.; Zhou, H.C. Photochromic Metal-Organic Frameworks: Reversible Control of Singlet Oxygen Generation. *Angew. Chem.-Int. Edit.* **2015**, *54*, 430–435. [[CrossRef](#)]
31. Chakarova, K.; Strauss, I.; Mihaylov, M.; Drenchev, N.; Hadjiivanov, K. Evolution of acid and basic sites in UiO-66 and UiO-66-NH<sub>2</sub> metal-organic frameworks: FTIR study by probe molecules. *Microporous Mesoporous Mater.* **2019**, *281*, 110–122. [[CrossRef](#)]
32. Klet, R.C.; Liu, Y.Y.; Wang, T.C.; Hupp, J.T.; Farha, O.K. Evaluation of Bronsted acidity and proton topology in Zr- and Hf-based metal-organic frameworks using potentiometric acid-base titration. *J. Mater. Chem. A* **2016**, *4*, 1479–1485. [[CrossRef](#)]
33. Butova, V.V.; Aboaraia, A.M.; Solayman, M.; Yahia, I.S.; Zahran, H.Y.; Abd El-Rehim, A.F.; Algarni, H.; Khabiri, G.; Soldatov, A.V. The joint effect of naphthalene-system and defects on dye removal by UiO-66 derivatives. *Microporous Mesoporous Mater.* **2021**, *325*, 111314. [[CrossRef](#)]
34. Strauss, I.; Chakarova, K.; Mundstock, A.; Mihaylov, M.; Hadjiivanov, K.; Guschanski, N.; Caro, J. UiO-66 and UiO-66-NH<sub>2</sub> based sensors: Dielectric and FTIR investigations on the effect of CO<sub>2</sub> adsorption. *Microporous Mesoporous Mater.* **2020**, *302*, 110227. [[CrossRef](#)]
35. Shepelenko, E.N.; Makarova, N.I.; Karamov, O.G.; Dubonosov, A.D.; Podshibakin, V.A.; Metelitsa, A.V.; Bren', V.A.; Minkin, V.I. Synthesis and Photochromic Properties of Asymmetric Dihetarylethenes Based on 5-methoxy-1,2-dimethylindole and 5-(4-bromophenyl)-2-methylthiophene. *Chem. Heterocycl. Compd.* **2014**, *50*, 932–940. [[CrossRef](#)]
36. Yang, X.L.; Ding, C.; Guan, R.F.; Zhang, W.H.; Feng, Y.; Xie, M.H. Selective dual detection of H<sub>2</sub>S and Cu<sup>2+</sup> by a post-modified MOF sensor following a tandem process. *J. Hazard. Mater.* **2021**, *403*, 123698. [[CrossRef](#)]
37. Du, Z.Y.; Li, B.L.; Jiang, C.; Sun, R.P.; Chen, S.W. Sorption of U(VI) on Schiff-base functionalized metal-organic frameworks UiO-66-NH<sub>2</sub>. *J. Radioanal. Nucl. Chem.* **2021**, *327*, 811–819. [[CrossRef](#)]
38. Petříček, V.; Dušek, M.; Palatinus, L. Crystallographic Computing System JANA2006: General features. *Z. Kristallog.* **2014**, *229*, 345–352. [[CrossRef](#)]
39. Brunauer, S.; Emmett, P.H.; Teller, E. Adsorption of Gases in Multimolecular Layers. *J. Am. Chem. Soc.* **1938**, *60*, 309–319. [[CrossRef](#)]
40. Morris, W.; Doonan, C.J.; Yaghi, O.M. Postsynthetic Modification of a Metal-Organic Framework for Stabilization of a Hemiaminal and Ammonia Uptake. *Inorg. Chem.* **2011**, *50*, 6853–6855. [[CrossRef](#)]
41. De Jong, J.J.D.; Browne, W.R.; Walko, M.; Lucas, L.N.; Barrett, L.J.; McGarvey, J.J.; van Esch, J.H.; Feringa, B.L. Raman scattering and FT-IR spectroscopic studies on dithienylethene switches—Towards non-destructive optical readout. *Org. Biomol. Chem.* **2006**, *4*, 2387–2392. [[CrossRef](#)]
42. Zheng, Y.T.; Sato, H.; Wu, P.Y.; Jeon, H.J.; Matsuda, R.; Kitagawa, S. Flexible interlocked porous frameworks allow quantitative photoisomerization in a crystalline solid. *Nat. Commun.* **2017**, *8*, 1–6. [[CrossRef](#)]
43. Hou, I.C.-Y.; Berger, F.; Narita, A.; Müllen, K.; Hecht, S. Proton-Gated Ring-Closure of a Negative Photochromic Azulene-Based Diarylethene. *Angew. Chem. Int. Ed.* **2020**, *59*, 18532–18536. [[CrossRef](#)]
44. Kobatake, S.; Terakawa, Y. Acid-induced photochromic system switching of diarylethene derivatives between P- and T-types. *Chem. Commun.* **2007**, *17*, 1698–1700. [[CrossRef](#)]